Embeddings of low-dimensional strange attractors: Topological invariants and degrees of freedom

Nicola Romanazzi[1], Marc Lefranc[2], and Robert Gilmore[1]
[1] *Physics Department, Drexel University, Philadelphia, Pennsylvania 19104, USA and*
[2] *Laboratoire de Physique des Lasers, Atomes, Molécules, UMR CNRS 8523, Centre d'Études et de Recherches Lasers et Applications, Université des Sciences et Technologies de Lille, F-59655 Villeneuve d'Ascq, France*
(Dated: February 1, 2008, *Physical Review E*: To be submitted.)

When a low dimensional chaotic attractor is embedded in a three dimensional space its topological properties are embedding-dependent. We show that there are just three topological properties that depend on the embedding: parity, global torsion, and knot type. We discuss how they can change with the embedding. Finally, we show that the *mechanism* that is responsible for creating chaotic behavior is an invariant of all embeddings. These results apply only to chaotic attractors of genus one, which covers the majority of cases in which experimental data have been subjected to topological analysis. This means that the conclusions drawn from previous analyses, for example that the mechanism generating chaotic behavior is a Smale horseshoe mechanism, a reverse horseshoe, a gateau roulé, an S-template branched manifold, ..., are not artifacts of the embedding chosen for the analysis.

I. INTRODUCTION

Chaotic time series have been generated by a large number of experiments. Typically a scalar time series is available, and a chaotic attractor must be generated from the scalar time series using some embedding procedure. The algorithm of choice is the time delay embedding [1, 2, 3] although differential embeddings, Hilbert transform embeddings, and singular value decomposition embeddings have also been used [4, 5].

The properties of embedded chaotic attractors have been analyzed along three distinct mathematical lines: geometric, dynamical, and topological. Geometric analyses involve computing various fractal dimensions [6]. Dynamical analyses involve computing Lyapunov exponents and the average Lyapunov dimension [7]. Topological analyses concentrate on the global topological properties of an attractor by studying how stretching and squeezing mechanisms organize the unstable periodic orbits embedded in the attractor [4, 5, 8, 9, 10].

In all approaches, it is assumed that the embedding adopted creates a diffeomorphism between the underlying (invisible) experimental attractor that generates the data and the embedded, or reconstructed, chaotic attractor [2, 3]. Since the geometric and dynamical measures (dimensions and exponents) are invariant under diffeomorphisms, in principle these real numbers are embedding-independent. In practice they are difficult to compute, and become increasingly difficult to compute as the length of the time series and/or the signal to noise ratio decreases. Further, there is no independent way to compute errors for the estimates of these real numbers. It was even shown in [11] that in some experimental data sets estimates of the fractal dimensions are diffeomorphism-dependent. Spurious Lyapunov exponents occur when the embedding dimension exceeds the dimension of the dynamical system. This has been addressed in [12, 13] but remains an open problem.

By constrast, topological analyses on three dimensional embeddings have been carried out with relatively short experimental data sets and are robust against noise. In addition, this analysis method is overdetermined. The stretching and squeezing mechanism creating the embedded chaotic attractor can be determined from a small number of unstable periodic orbits and used to predict the topological organization of all remaining orbits. These predictions (linking numbers, relative rotation rates) either agree or do not agree with those for orbits extracted from the embedded chaotic attractor. In the latter case the model describing stretching and squeezing must be rejected.

What has never been satisfactorily understood is the relation between the topological properties of the underlying (invisible) experimental attractor that generates the data and the chaotic attractor that has been constructed through an embedding of the data. We illustrate this difficulty with two examples. (1) The Lorenz attractor [14] is described by variables $(x(t), y(t), z(t))$. One three-dimensional embedding is the obvious one: $(X_1, X_2, X_3) = (x, y, z)$. The chaotic attractor in this embedding is invariant under rotations: $(X_1, X_2, X_3) \to (-X_1, -X_2, X_3)$. On the other hand, if a single variable is observed (either $x(t)$ or $y(t)$) [15] the chaotic attractor created through the differential embedding $(X_1, X_2, X_3) = (x, \dot{x}, \ddot{x})$ will exhibit inversion symmetry $(X_1, X_2, X_3) \to (-X_1, -X_2, -X_3)$ [16, 17]. (2) The chaotic behavior of Bénard-Marangoni fluid convection in a square cell [18] was modeled by a periodically driven Takens-Bogdanov nonlinear oscillator [19]. This model was studied using a time delay mapping of the form $(X_1, X_2, X_3) = (x(t), \dot{x}(t), x(t-\tau))$ [20]. For a range of values of the time delay τ, $\tau_1 < \tau < \tau_2$, the image of the data under this mapping exhibits self intersections and the mapping is therefore not an embedding (technically, it is an immersion) [20, 21]. For $\tau < \tau_1$ and $\tau_2 < \tau$ the mapping is an embedding. The topological organization

of the unstable periodic orbits under the two embeddings is different, so the global topological structure of the two embedded attractors is not equivalent [21].

This discussion brings us to the crucial question: When topological information about a chaotic attractor is determined from a three-dimensional embedding of the chaotic attractor, what part of that information is embedding-dependent and what part is embedding-independent? In this work we answer this question for a large class of chaotic attractors. These consist of all chaotic attractors of "genus-one" type [22, 23]: their natural phase space is equivalent to a torus. This includes the chaotic attractor discussed in the example (2) above. The answer is that the "mechanism" (defined in Sec. V below) is independent of embedding. Further, the topological organization of all periodic orbits in the attractor can differ in a very limited number of ways (parity, global torsion, and knot type, see Sec. IV below). This crucial question remains open for chaotic attractors whose natural phase space is a torus of genus g ($g > 1$). This includes the Lorenz attractor as well as many other chaotic attractors [22, 24]. It also remains open for all higher-dimensional (hyper-)chaotic attractors.

II. ASSUMPTIONS

We make the following assumptions:

1. A deterministic process (e.g., laser equations, Navier-Stokes equations) acts to generate an experimental chaotic attractor that is three-dimensional. A single variable (e.g., laser intensity, fluid surface height) is measured.

2. At least one embedding of this scalar time series in $\mathbb{R}^3$ can be constructed. This embedding creates a diffeomorphism between the original experimental chaotic attractor and the embedded or "reconstructed" chaotic attractor.

3. The embedded chaotic attractor is of genus-one type: that is, it can be enclosed in a genus-one bounding torus [22, 23].

Some remarks about these assumptions are in order. We assume in (1) that there is an experimental chaotic attractor and that it is three dimensional. By three-dimensional we mean explicitly that there is a three dimensional manifold in the phase space that contains the attractor. We require this assumption on dimension because, at the present time, topological analysis methods based on templates are only applicable to three dimensional chaotic attractors, that is, those that that exist in three-dimensional manifolds. The assumption that the deterministic process generates a low-dimensional attractor is also strong: the Navier-Stokes and the full laser equations are partial differential equations rather than sets of ordinary differential equations, and act in Hilbert spaces rather than finite dimensional phase spaces [25].

Assumption (2) is necessary because the Whitney embedding theorem [1] and its dynamical variants [2, 3] only guarantee that the three-dimensional manifold containing the chaotic attractor can be embedded into a space of sufficiently high dimension ($6 = 2 \times 3$), but do not ensure that it can be done into a three-dimensional phase space. In practice, whether this assumption holds can be tested *a posteriori* by verifying that the topological invariants measured are consistent with a single two-dimensional branched manifold. The diffeomorphism property that is assumed of the mapping is the standard assumption for all approaches to analysis of embedded data [2, 3].

Assumption (3) is crucial for our result. It allows us to reduce the problem of the inequivalence of embeddings of chaotic attractors to the problem, already solved [26], of the equivalence classes of diffeomorphisms of the solid torus into the three-dimensional euclidean space R^3. In the higher genus case (e.g., Lorenz attractor) the spectrum of inequivalent diffeomorphisms (embeddings) of these attractors is related to the spectrum of inequivalent diffeomorphisms of the higher genus tori to themselves, which remains to be studied.

III. PRELIMINARY REMARKS

We begin by recalling that diffeomorphisms map periodic orbits to periodic orbits. If $\mathbf{x}(t)$ is a point on a periodic orbit so that $\mathbf{x}(t+T) = \mathbf{x}(t)$, then under a diffeomorphism that takes $\mathbf{x} \to \mathbf{y}$, $\mathbf{y}(t) = \mathbf{y}(t+T)$. This means that periodic orbits are neither created nor annihilated by diffeomorphisms. In particular, the spectrum of periodic orbits associated with ("in") a chaotic attractor is an invariant of diffeomorphisms. On the other hand their topological organization, as encoded by their topological invariants (linking numbers, relative rotation rates) could change under diffeomorphism.

We will describe exactly how these topological invariants can change under diffeomorphism when the phase space containing the chaotic attractor is a torus $D^2 \times S^1$, where D^2 is a disk in the plane ($D^2 \subset R^2$) and S^1 is parameterized by ϕ, usefully considered as a phase angle mod 2π. In this phase space trajectories can be expressed in the form $(x(t), y(t), \phi(t))$. This class includes nonautonomous dynamical systems such as the periodically driven Duffing, van der Pol, and Takens-Bogdanov nonlinear oscillators where ϕ and t are linearly related, and autonomous dynamical systems whose phase space projection $(x, \dot{x})$ exhibits a 'hole in the middle' (e.g., Rössler system [27] at $(a, b, c) = (0.398, 2.0, 4.0)$). It includes other autonomous dynamical systems with a hole in the middle that is present but obscured by simple projections (e.g., Rössler system at $(a, b, c) = (0.398, 2.0, 13.3)$). For this class of systems the phase $\phi = \phi(t)$ is a monotonic function of the time t. This discussion explicitly excludes attractors of genus $g \geq 2$ with two or more 'holes in the middle', such as the Lorenz attractor.

In the work to follow we seek a discrete enumeration

of embeddings, or diffeomorphsims, of strange attractors. To achieve this end it is necessary to "mod out" continuous degrees of freedom associated with diffeomorphisms. To do this we introduce the idea of isotopy. Two embeddings f_0 and f_1 are isotopic is there is a one parameter family of mappings, $f(s)$, with $f(0) = f_0$, $f(1) = f_1$ and $f(s)$ is an embedding for *all* s, $0 \leq s \leq 1$. Such a family of embeddings merely deforms the phase space smoothly. The topological organization of periodic orbits is unchanged under isotopy. For if two orbits intersected during the deformation from $s = 0$ to $s = 1$ the uniqueness theorem would be violated and the mapping $f(s)$ (for some s) would not be a diffeomorphism. For this reason isotopic mappings are in some sense equivalent. The sense is that all topological indices for orbits in a strange attractor are the same for all embeddings in the same isotopy class.

Our problem therefore reduces to (1) classifying the set of isotopy classes of diffeomorphisms $D^2 \times S^1 \to D^2 \times S^1$, (2) classifying the set of isotopy classes of diffeomorphisms $D^2 \times S^1 \to R^3$, and (3) determining how topological invariants change from one class to another. The first two parts of this program are resolved in Secs. IVa and IVb. The third part is discussed in Secs. V and VI. A more detailed exposition of these points is presented in Appendix A.

IV. EMBEDDINGS OF A TORUS

Diffeomorphisms of the torus fall into two broad classes: intrinsic and extrinsic [26, 28]. Intrinsic diffeomorphisms are mappings of the torus to itself "as seen from the inside." Specifically, they are mappings $D^2 \times S^1 \to D^2 \times S^1$. Extrinsic diffeomorphisms describe how the torus sits in R^3. They are mappings $D^2 \times S^1 \to R^3$. Intrinsic diffeomorphisms are responsible for two of the three degrees of freedom mentioned in the abstract and introduction: parity and global torsion. Extrinsic diffeomorphisms are responsible for the first two and in addition the third: knot type.

A. Intrinsic Diffeomorphisms.

These also fall into two classes: those that are isotopic to the identity and those that are not.

Isotopic to the Identity. Diffeomorphisms that are isotopic to the identity smoothly deform the phase space. Therefore they do not change the topological organization of the periodic orbits in it. Under these diffeomorphisms the topological invariants of periodic orbits remain unchanged.

Not Isotopic to the Identity. Mappings of the torus to itself that are not isotopic to the identity have been classified [26]. The idea is as follows. On the two-dimensional surface $T^2 = \partial(D^2 \times S^1)$ that is the boundary of the solid torus it is possible to construct two circles that cannot be deformed to a point, as shown in Fig. 1. We orient both. The longitude is oriented along the direction of the dynamical system flow. The meridian bounds a disk that can be used as a Poincaré surface of section. It is oriented according to the right hand rule. Up to isotopy (the class of diffeomorphisms considered in the preceeding paragraph) the inequivalent diffeomorphisms of the torus to itself are classified by their action on the longitude and meridian by the matrix [26]

$$\begin{bmatrix} 1 & n \\ 0 & \pm 1 \end{bmatrix} \tag{1}$$

The integer n describes the number of rotations of the longitude about the core (center line) of the torus as the phase angle ϕ increases from 0 to 2π. The integer ± 1 indicates whether the diffeomorphism preserves or reverses the orientation of the meridian. We identify ± 1 with parity and n with global torsion in Sec. V.

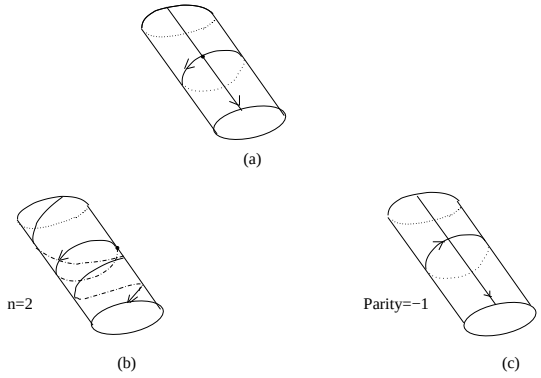

FIG. 1: (a) Two nonisotopic circles are drawn on the surface of the solid torus containing a chaotic attractor. The longitude is oriented along the direction of the flow. The meridian is oriented by the right hand rule. The solid torus is mapped diffeomorphically to a torus with (b) $n = 2$ or (c) negative parity.

Remark. The matrices presented in Eq.(1) are group operations. Diffeomorphisms of the torus to itself form a group. The subset that is isotopic to the identity forms a subgroup that is invariant in the larger group. The quotient of these two groups therefore forms a group. This group is discrete. It is generated by two operations, represented by the matrices

$$\begin{bmatrix} 1 & 1 \\ 0 & 1 \end{bmatrix} \qquad \text{and} \qquad \begin{bmatrix} 1 & 0 \\ 0 & -1 \end{bmatrix} \tag{2}$$

The first describes the generator that produces a uniform rotation along the axis of the torus: $((x+iy), \phi) \to ((x+iy)e^{i\phi}, \phi)$. The second generator produces the effect of looking into a mirror: $(x, y, \phi) \to (x, -y, \phi)$. This coset decomposition says simply that every intrinsic diffeomorphism can be constructed by composing a diffeomorphism isotopic to the identity with one from the

discrete group whose matrix representation is given in Eq.(1).

B. Extrinsic Diffeomorphisms.

The mapping of $D^2 \times S^1$ into R^3 shown in Fig. 2(a) is called the 'natural embedding' [26]. One natural embedding of a chaotic attractor with coordinates $(x_1(\phi), x_2(\phi), \phi)$ in $D^2 \times S^1$ into R^3 is $(X(t), Y(t), Z(t))$, with $t = \phi$ and $X = (R - x_1)\cos\phi$, $Y = (R - x_1)\sin\phi$, and $Z = x_2$. This is an embedding provided the circle is "bigger" than the attractor. Specifically, if the radius of the disk D^2 containing the attractor is a, so that $x_1^2(\phi) + x_2^2(\phi) < a^2$ for all ϕ, then $R > a$ guarantees that no self-intersections occur in the natural embedding.

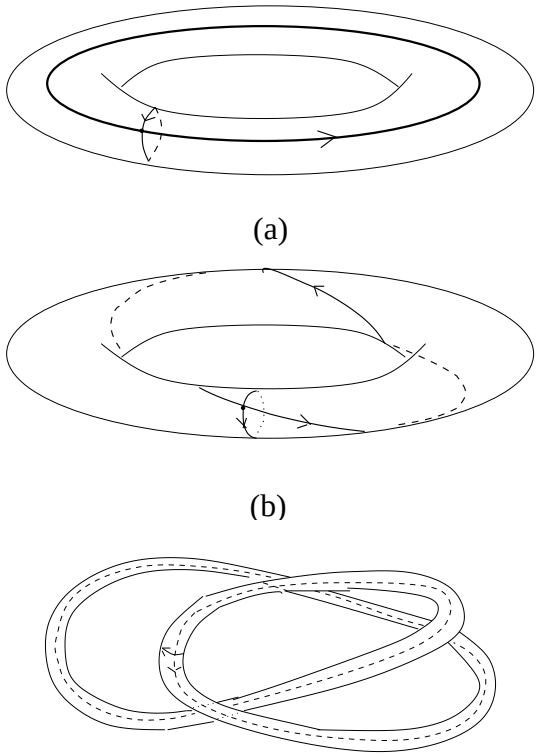

FIG. 2: (a) The torus $D^2 \times S^1$ of Fig. 1(a) is embedded in a natural way in R^3. In this embedding the core of the torus is a circle of radius R. the torus can also be mapped into R^3 with a nonzero framing index f. The framing index is $+1$ in the embeddings (b) and (c).

The circle is the simplest knot in R^3. Other knots in R^3 can be used as central curves for other extrinsic embeddings. The knot $\mathcal{K}$ has coordinates $\mathbf{K}(\phi) = (K_1(\phi), K_2(\phi), K_3(\phi))$ with $\mathbf{K}(\phi) = \mathbf{K}(\phi + 2\pi)$. As with any smooth space curve [29] this knot has a moving coordinate system (*repere mobile*) with orthogonal unit vectors $\mathbf{t}(\phi), \mathbf{n}(\phi), \mathbf{b}(\phi)$. The section of a chaotic attractor in $D^2 \times S^1$ at phase angle ϕ is lifted into the plane in R^3 perpendicular to the tangent vector $\mathbf{t}(\phi)$ at $\mathbf{K}(\phi)$ by the mapping $(x_1(\phi), x_2(\phi), \phi) \rightarrow \mathbf{K}(\phi) + x_1(\phi)\mathbf{n}(\phi) + x_2(\phi)\mathbf{b}(\phi)$. This mapping is an embedding provided there are no self intersections. This is guaranteed provided two conditions are satisfied [30]:

Local condition: The radius of curvature of $\mathcal{K}$ is everywhere greater than a.

Global condition: The curve $\mathcal{K}$ is "big enough." This means specifically that all nonzero local minima of $|\mathbf{K}(\phi_1) - \mathbf{K}(\phi_2)|$ are larger than $2a$.

An important integer is associated with each knot $\mathcal{K}$. This is its framing index, f [26]. It describes how many times the vectors $\mathbf{n}$ and $\mathbf{b}$ wind around $\mathbf{t}$ as the knot is traversed. Specifically, it is the gauss linking number of two closed curves in R^3. One closed curve is the knot itself. The other is obtained by displacing it a small distance along the normal vector. Its coordinates are given by setting $(x_1(\phi), x_2(\phi), \phi) = (1, 0, \phi)$ in the mapping above. We use this integer in Sec. VI to describe the problems of the delay embeddings of the fluid data presented in Sec. I, Example (2) (embedding of Benard-Marangoni fluid data). Embeddings of the torus into R^3 with framing index $f = +1$ are shown in Fig. 2(b) and (c).

Remark. As Fig. 2 shows, choice of a knot in R^3 for the center curve of the embedded torus is independent of the choice of the framing index of the embedded torus. The knot type of the center curve is one degree of freedom of embeddings of a genus-one torus into R^3. Two other degrees of freedom, the framing index (which is equivalent to global torsion) and parity have already been encountered in diffeomorphisms $D^2 \times S^1 \rightarrow D^2 \times S^1$.

Remark. It is pedantically more accurate to describe extrinsic embeddings as diffeomorphisms $D^2 \times S^1 \rightarrow D^2 \times S^1 \subset R^3$. In the remainder we forgo this mathematical precision.

V. MECHANISMS

Chaotic attractors in three dimensional spaces are characterized by the spectrum and topological organization of their unstable periodic orbits (UPOs) [4, 5]. The topological organization of the periodic orbits is summarized by a knot holder (also called a branched manifold or a template) [31, 32]. The spectrum of UPOs in the attractor is a subset of all the orbits contained in the knot holder. This subset is specified by a basis set of orbits [33]. The knot holder that describes an embedded chaotic attractor is identified by extracting a rather small set of orbits from the attractor and determining their topological organization [10]. As a result, knot holders are invariant under diffeomorphisms isotopic to the identity, since they are derived from the topological indices of periodic orbits, which do not change under isotopy. Knot holders can differ only by the indices that describe the distinct equivalence classes of diffeomorphisms. These are: the

parity index ± 1, the global torsion n, and the knot type of the embedding into R^3, including the framing index f. Further, as the spectrum of UPOs in a chaotic attractor is a diffeomorphism invariant, every embedding of a chaotic attractor has the same basis set of orbits.

A knot-holder has as many branches as the number of symbols required to uniquely identify the unstable periodic orbits in the attractor. This number, as well as the symbolic name of each periodic orbit, can be determined by constructing a generating partition [34, 35, 36, 37, 38]. Techniques have also been developed to construct the knot-holder without prior knowledge of a symbolic encoding, by searching directly for the simplest template with a set of orbits isotopic to the experimental one [5, 39, 40]. A generating partition can then be constructed from this information [39, 40, 41].

A knot-holder has one or more branch lines. Two or more branches leave from each branch line ("stretching process"), and two or more branches meet at each branch line ("squeezing process"). Since knot holders are surrogates for chaotic attractors [31, 32], we regard information about which branches leave each branch line and which meet at each branch line as describing the mechanism generating chaos.

Chaotic attractors in a torus (genus one) possess a single branch line [22], which may be an interval (Rössler and Duffing attractors) or a circle (van der Pol attractor). For attractors in $D^2 \times S^1$ by "mechanism" we mean explicitly the order in which branches leave the branch line (left to right) or circle (clockwise or counterclockwise) and the order in which the branches are squeezed together when they return to the branch line (front to back) or circle (inside to outside) [9]. In the genus one case, mechanism describes how the branch curve (line, circle) is folded back into itself in one forward iteration. The return flow, from the output side of the branch line (lines c to d in Fig. 3(a)) to the input side (lines a to b in Fig. 3(a)) is assumed to preserve order. The "mechanism" is shown within the dashed rectangle of Fig. 3. The part of the branched manifold describing the flow from b to c is the part of the branched manifold that describes stretching (the divergence of branches A and B) and squeezing (the joining of branches A and B). This is the part of the branched manifold describing "mechanism." This knot-holder has only one branch line. We have shown four in Fig. 3 to emphasize the various roles played by that branch line.

Knot-holders for chaotic attractors in a genus-one torus are classified by a pair of matrices [4, 5, 8, 10]. If n symbols are required to label periodic orbits, one matrix (the "template matrix") is an $n \times n$ matrix and the other ("array matrix" or "joining matrix") is a $1 \times n$ matrix. These two matrices are shown in Fig. 4 for two particular knot-holders. One (Fig. 4(b)) is the outside to inside scroll template with three branches, which has been observed in (embeddings of) experimental data from lasers [42, 43, 44] and from neurons [50]. The other (Fig. 4(a)) is the inside-to-outside gateau roulé. The diagonal matrix elements T_{ii} of the template matrix describe the local torsion (measured in units of π) for branch i. The off-diagonal matrix elements $T_{ij} = 2 \times Link(i,j)$ are twice the linking numbers of the period-one orbits in branches i and j. The array matrix describes the order in which the branches are glued together at the branch line: the smaller the integer entry, the further from the viewer in the projection.

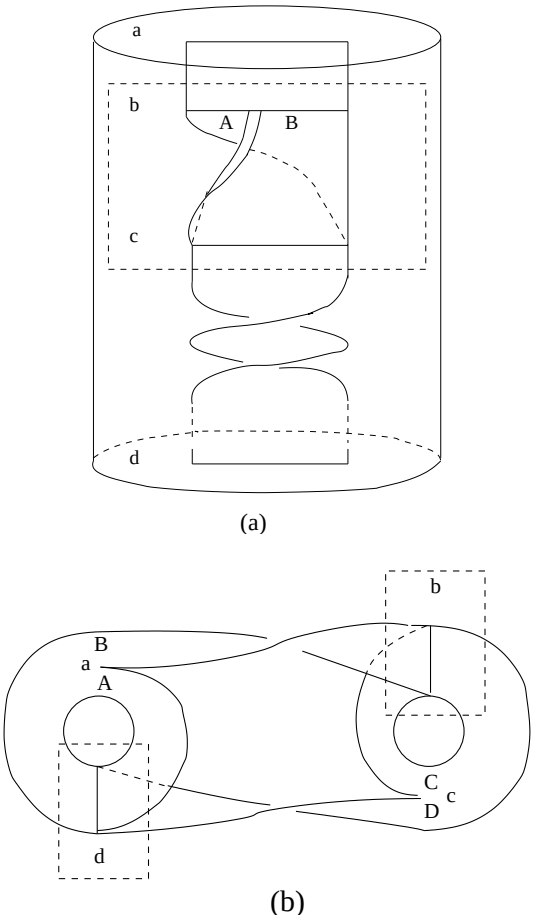

FIG. 3: (a) Knot holder for the Rössler attractor, shown inside a torus $D^2 \times S^1$. The flow enters at a, is split at b, joined at c, and "leaves" at d. Periodic boundary conditions identify a and d. We also identify b with a and c with d. (b) Knot holder for the Lorenz attractor, shown inside a genus-three torus. Branches A and B split at a while C and D split at c. Branches C and B join at b while D and A join at d. In both cases the mechanism is shown within the dashed box (a) or boxes (b).

Mechanisms that differ by being mirror images or by having integer global torsion are represented by closely related matrices. In the opposite parity case, the mirror image knot holder has all integer entries with opposite signs. In the case of global torsion n, the even integer $2n$ is added to all entries in the template matrix. The matrices that describe these two variations of the gateau-roulé mechanism [c.f. Fig. 4(b)] are

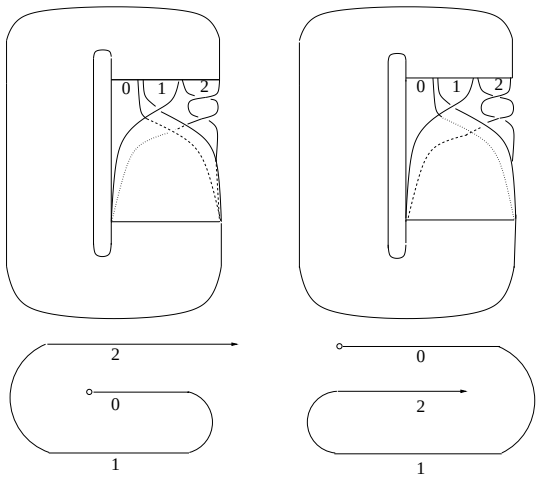

Branch	Matrices	Branch	Matrices
0	$\begin{bmatrix} 0 & 0 & 2 \\ 0 & 1 & 2 \\ 2 & 2 & 2 \end{bmatrix}$	0	$\begin{bmatrix} 0 & 0 & 0 \\ 0 & 1 & 2 \\ 0 & 2 & 2 \end{bmatrix}$
1		1	
2		2	
	$\begin{bmatrix} 1 & 2 & 0 \end{bmatrix}$		$\begin{bmatrix} 0 & 2 & 1 \end{bmatrix}$

FIG. 4: Three-branch knot-holder for an (a) inside-to-outside and (b) outside-to-inside "jelly roll" mechanism. the template matrices and arrays that describe these branched manifolds algebraically are also shown.

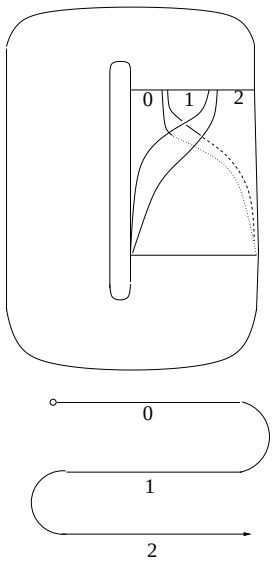

Branch	Matrices
0	$\begin{bmatrix} 0 & 0 & 0 \\ 0 & 1 & 0 \\ 0 & 0 & 0 \end{bmatrix}$
1	
2	
	$\begin{bmatrix} 0 & 1 & 2 \end{bmatrix}$

FIG. 5: Three-branch knot-holder for an S-mechanism, along with its template matrix and joining array.

Branch	Parity	Global Torsion n
0	$\begin{bmatrix} 0 & 0 & 0 \\ 0 & -1 & -2 \\ 0 & -2 & -2 \end{bmatrix}$	$\begin{bmatrix} 2n & 2n & 2n \\ 2n & 2n+1 & 2n+2 \\ 2n & 2n+2 & 2n+2 \end{bmatrix}$
1		
2		
	$\begin{bmatrix} 0 & -2 & -1 \end{bmatrix}$	$\begin{bmatrix} 0 & 2 & 1 \end{bmatrix}$

(3)

Embeddings with nontrivial knot type do little to alter the matrices that describe the mechanism that generates chaotic behavior [21]. Nontrivial knot type may change parity and add global torsion, depending on the framing [26] of the knot (see Sec. IV).

To be explicit, a mechanism that generates chaos requiring three symbols can be of two types: a scroll mechanism (Fig. 4) or an "S" mechanism. The template for the latter is shown in Fig. 5, along with its description in terms of matrices.

If one embedding of data reveals a scroll template, all embeddings will reveal a scroll mechanism. If on the other hand one embedding reveals an S mechanism, every other embedding of these data will also reveal an S mechanism. This is true because no transformation involving sign changes or addition of global torsion [c.f., Eq. (3)] can change the description given in Fig. 4 to the description given in Fig. 5. The mechanism (scroll or S) is an invariant of embeddings.

Similarly, a horseshoe mechanism $\mathcal{H}(n,\epsilon)$ will be described in all embeddings by template matrices

	Branch	Matrices
Horseshoe with Parity and Global Torsion	0	$\begin{bmatrix} 2n & 2n \\ 2n & 2n+\epsilon \end{bmatrix}$
	1	
		$\begin{bmatrix} 0 & \epsilon \end{bmatrix}$

(4)

with $\epsilon = \pm 1$ and n indicating parity and global torsion or framing index, respectively. Matrices (4) describe all possible templates with two branches folding over each other. A mechanism identified as a horseshoe in one embedding is a horseshoe in any embedding.

VI. TOPOLOGICAL INDICES

Relative rotation rates are the natural topological index for periodic orbits in the torus $D^2 \times S^1$ [8]. Linking numbers are the natural topological index for periodic orbits in R^3.

Assume A and B are two periodic orbits in some embedding in the torus $D^2 \times S^1$, and that their relative rotation rates are $R_{ij}(A,B)$. These fractions are invariant

under diffeomorphisms isotopic to the identity. Under diffeomorphisms $D^2 \times S^1 \to D^2 \times S^1$ with global torsion n, or with parity -1, that map $A \to A'$ and $B \to B'$

$$\begin{array}{lrll} \text{Global torsion} = & n & R_{ij}(A',B') & = R_{ij}(A,B) + n \\ \text{Parity} = & -1 & R_{ij}(A',B') & = -R_{ij}(A,B) \end{array}$$

Diffeomorphisms $D^2 \times S^1 \to R^3$ map $A \to A''$ and $B \to B''$. For these closed curves in R^3 it is possible to compute both relative rotation rates and linking numbers. Under the natural embedding [8] (c.f., Fig. 2)

$$R_{ij}(A'',B'') \ \to \ R_{ij}(A,B)$$

Under an embedding into R^3 with framing index f

$$R_{ij}(A'',B'') \ \to \ R_{ij}(A,B) + f$$

In all cases the linking numbers of A'' and B'' in R^3 are the sum of their relative rotation rates [8]:

$$L(A'',B'') = \sum_{i=1}^{p_A} \sum_{j=1}^{p_B} R_{ij}(A'',B'')$$

where $p_A = p_{A''}$ is the period of orbits A and A'', and similarly for B. The dependence of the linking number of A'' and B'' on the framing index f is

$$L_f(A'',B'') = L_0(A'',B'') + f p_A p_B$$

The framing index f for embeddings $D^2 \times S^1 \to D^2 \times S^1 \subset R^3$ can be considered, for all practical purposes, as equivalent to the global torsion n for embeddings $D^2 \times S^1 \to D^2 \times S^1$.

VII. PERESTROIKAS

Up to this point the discussion has concentrated on embeddings of a single attractor. Usually experiments that generate chaotic attractors are carried out over a range of control parameter values in an effort to create the equivalent of a bifurcation diagram. In this section we discuss fixed embeddings of a family of attractors and the dual process: families of embeddings of a single attractor.

The first topological analysis of a family of chaotic attractors was carried out in [45]. A single embedding was used to analyze many data sets from lasers with saturable absorbers operated with three different absorbers and under various operating conditions. This analysis revealed that through all these changes the underlying branched manifold never changed: it was only the basis set of orbits that changed [33, 45]. Results for an NMR laser [46] and a nonlinear vibrating string [47] were the same. Subsequently, studies of the periodically driven Duffing oscillator [48], CO_2 lasers with modulated losses [39, 49], an Nd-doped YAG laser[42], an Nd-doped fiber laser [43, 44], and sensory neurons [50] showed that the underlying branched manifold was a "gateau roulé" or "jelly roll" branched manifold [4, 5], and that under variation of the modulation frequency the flow was directed to branches of this branched manifold with systematically increasing torsion.

In light of the results presented in the preceeding sections, these conclusions are embedding-independent: they would have been reached using any embedding. First, the variation of torsion with control parameters was observed using a fixed embedding, hence is due to physical effects and not to the choice of embedding. Within a fixed-embedding study, the standard horseshoe $\mathcal{H}(0,1)$ is topologically distinct from a "reverse" horseshoe $\mathcal{H}(1,-1)$ (as observed in [42]). Second, the spiral structure that globally describes attractors observed at different control parameters values would not have been affected if an embedding with different knot type, torsion and parity had been chosen.

It is often the case that families of mappings are studied in an effort to identify an optimum embedding. The method of minimum mutual information [51] was developed for precisely this reason. The first systematic study of the way the topological properties of an embedded attractor can depend on the embedding, or change with the embedding parameters, was carried out in [21]. This is the example (2) summarized in the Introduction. Mappings with a delay $\tau < \tau_1$ provided embeddings, as did mappings with $\tau > \tau_2$. In both cases, changing the delay τ by a little had no effect on the topological indices of the periodic orbits. In both cases the torus embedded in R^3 wound around a vertical axis three times before closing. In the transition from one regime of embeddings to the other all relative rotation rates changed by ± 2 (depending on whether the time delay τ increases or decreases). In the interval $\tau_1 < \tau < \tau_2$ the mapping exhibited self intersections, of the type indicated by the arrows in Fig. 2(c). The knot type of the embedding into R^3 remained unchanged but its framing in R^3 changed. Further, the change was by an even integer. This is a signature for framing changes caused by change in handedness of writhe [5].

VIII. SUMMARY AND CONCLUSIONS

When a low dimensional chaotic attractor is embedded in a three dimensional space, its topological properties depend on the embedding. We show that, for a large class of low dimensional attractors there are three topological properties that are embedding-dependent and one that is embedding-independent. The embedding-dependent properties are: parity, global torsion, and knot type. In the latter case (of mappings $D^2 \times S^1 \to R^3$), the framing index is the global torsion. The embedding-independent property is the mechanism that acts in phase space to create the chaotic attractor. Mechanism is defined in Fig. 3 in terms of branched manifolds. The class of chaotic attractors for which these results hold in-

cludes all genus-one attractors: those whose phase space is equivalent (diffeomorphic) to a torus $D^2 \times S^1$. This class includes the Rössler attractor, periodically driven two-dimensional nonlinear oscillators such as the Duffing, van der Pol, and Takens-Bogdanov attractors, and most of the experimentally generated chaotic attractors that have been studied by topological methods. The principal result is that any single embedding of a three dimensional attractor in this class suffices to determine the mechanism that has generated the chaotic data. This class does not include the Lorenz attractor and other attractors with more than one "hole in the middle."

APPENDIX A: CLASSIFICATION OF EMBEDDINGS OF $D^2 \times S^1$ INTO R^3.

1. Introduction

In this appendix, we provide the interested reader with more details about how embeddings of genus-one attractors can be classified in terms of knot type, torsion and parity.

Assume that two embeddings Ψ_1 and Ψ_2 of a chaotic attractor are possible. The simplest case is when Ψ_1 and Ψ_2 are isotopic: one embedding can be deformed continuously into the other. Equivalence of the topological properties of the two embeddings then trivially follows from the invariance of the topological indices of closed curves with respect to smooth deformations that do not induce self-intersections.

When Ψ_1 is not isotopic to Ψ_2, we exploit the assumption that the original strange attractor can be enclosed in a genus-one torus. We first note that a diffeomorphism (or homeomorphism) mapping the original attractor to a reconstructed attractor is defined on neighborhoods of these two strange sets, and can easily be extended to a diffeomorphism (or homeomorphism) between solid tori contained in these neighborhoods and enclosing the attractors.

Since isotopic embeddings are equivalent, determining how topological properties of two genus-one embeddings of an attractor can differ thus simply amounts to studying isotopy classes of embeddings of $D^2 \times S^1$ into $\mathbb{R}^3$. There are two levels in the classification of these isotopy classes, because there are two ways in which two embedded solid tori can be non-isotopic. The first level is extrinsic and deals with how the core of the solid torus is embedded in $\mathbb{R}^3$. When shrunk to their respective cores, two solid tori are isotopic if they have the same knot type. The second level is intrinsic and deals with how torus boundaries $\partial(D^2 \times S^1) = T^2$ are mapped to torus boundaries. Two embeddings such that the cores of the embedded tori have the same knot type can still be non-isotopic if the homeomorphism mapping the boundary of one torus to the boundary of the other is not isotopic to identity.

From this classification, we finally conclude that there are three degrees of freedom in which two embeddings of a genus-one attractor into R^3 can differ: knot type (extrinsic level), torsion and parity (at both extrinsic and intrinsic levels).

2. Extrinsic level: knot type

A necessary condition for two embeddings of a manifold M to be isotopic is that their restrictions to a given submanifold $M' \subset M$ are isotopic [26]. In particular, consider the core of the solid torus $D^2 \times S^1$, i.e., the submanifold $\mathcal{C} = \{B\} \times S^1$ with a base point $B \in D^2$. Two isotopic embeddings of $D^2 \times S^1$ into $\mathbb{R}^3$ must embed $\mathcal{C}$ into $\mathbb{R}^3$ isotopically. Since $\mathcal{C}$ is an embedding of S^1 into $D^2 \times S^1$, embeddings of C in $\mathbb{R}^3$ can be classified as embeddings of S^1 in $\mathbb{R}^3$, i.e., as ordinary knots. Two torus cores are thus isotopic if and only if they have the same knot type. Conversely, two embedded solid tori whose cores are knotted in different ways cannot be isotopic.

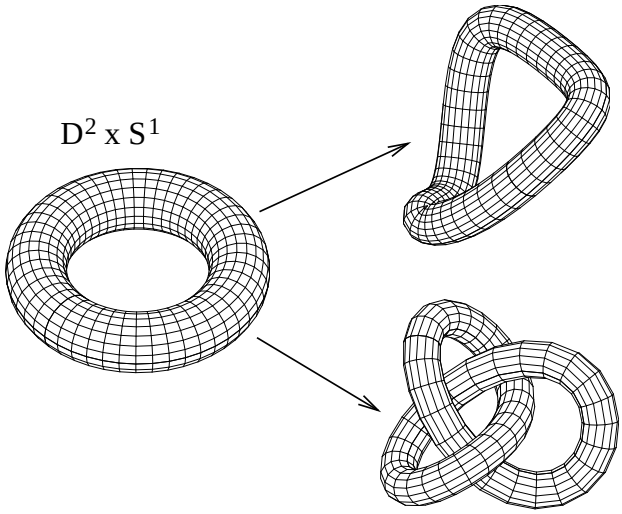

FIG. 6: Two embeddings of $D^2 \times S^1$ as solid tori in $\mathbb{R}^3$ cannot be isotopic if their cores are not isotopic.

The actual situation (embedding) of tori in $\mathbb{R}^3$, as described by the knot type of the torus core, is called the extrinsic structure [28]. Every (tame) knot can be used as a centerline for a torus that is embedded in $\mathbb{R}^3$.

Assume that two embedded solid tori have isotopic cores. This allows us to superimpose the boundaries of the two solid tori by isotopy deformations. This does not imply that the two embeddings are isotopic. However, this indicates that we can now study the classification of embeddings at an intrinsic level, by considering mappings of the solid torus into itself and forgetting about position in $\mathbb{R}^3$ (looking now at the torus from the inside rather than from the outside). Thus, knot type of the torus core captures all information about isotopy classes at the extrinsic level.

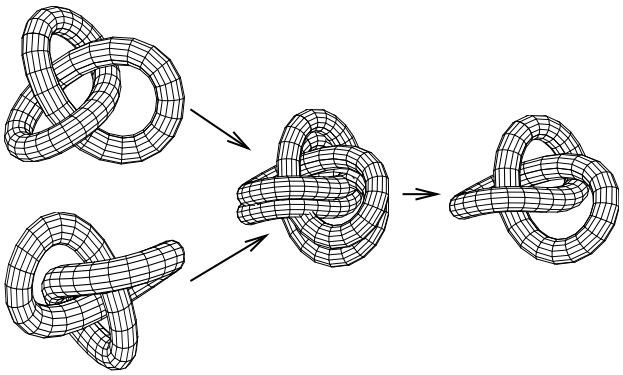

FIG. 7: The boundaries of two embedded solid tori with isotopic cores can be superimposed by isotopy deformations.

3. Intrinsic level: global torsion and parity

We consider now two embeddings Ψ_1 and Ψ_2 of $D^2 \times S^1$ such that the cores of the embedded solid tori are isotopic and their boundaries are superimposed (Fig. 7). A necessary condition for the two embeddings to be isotopic is that their restriction to the boundary of the tori are isotopic, as with any submanifold. This condition is equivalent to requiring that the restriction of $(\Psi_1)^{-1}\Psi_2$ to the boundary of the first torus is isotopic to identity. It is also a sufficient condition because a homeomorphism of the torus that has its restriction isotopic to identity is isotopic to identity [26]. Thus, we are left with studying isotopy classes of homeomorphisms of the boundary $\partial(D^2 \times S^1) = T^2$ into itself.

The group of homeomorphisms of this surface to itself modulo isotopically equivalent embeddings is called the mapping class group and is equivalent to the modular group of 2×2 matrices $GL(2;Z) = \begin{bmatrix} a & b \\ c & d \end{bmatrix}$, with a, b, c, d integer and $ad - bc = \pm 1$ [26]. This group describes how closed curves $S^1 \subset T^2$ are mapped to closed curves in T^2 under the homeomorphism. The description is given in terms of the basis set of (two) loops for the homotopy group of T^2. These two cycles are the meridian and the longitude. The meridian can be regarded as the small loop that goes around a tire "the short way" and the longitude as a long loop that goes around the tire "the other way" (c.f., Fig. 1(a)). At the topological level (homeomorphism) they are more or less equivalent. At the level of dynamical systems they are not. The meridian bounds a disk that lies inside $D^2 \times S^1$ and can be taken as everywhere transverse to the flow that generates the strange attractor or its embedding. This disk can be chosen as a global Poincaré surface of section. The longitude can be chosen in the direction of the flow. By restricting to the topology underlying the dynamics, we investigate the class of inequivalent homeomorphisms of the torus boundary into itself. These are described by modular group operations of the form

$$M = \begin{bmatrix} 1 & n \\ 0 & \epsilon \end{bmatrix} \tag{A1}$$

with $\epsilon = \pm 1$. We interpret the integer n as the number of times the longitude links the core of the solid torus $D^2 \times S^1$. Dynamically, n is the global torsion of the embedding. The sign $\epsilon = \pm 1$ identifies the parity of the torus homeomorphism.

A point has to be made regarding parity. The mirror image of an embedding is also an embedding, which differs from the original embedding only by orientation. In the mirror image of an embedding, all the topological invariants are multiplied by -1. Since an embedding and its mirror image cannot be isotopic because orientation is preserved under isotopy (orientation cannot change without inducing self-intersections at some stage of the deformation), parity has to be taken account when classifying embeddings of solid tori into $\mathbb{R}^3$.

Mirror image transformations act both at the extrinsic and intrinsic levels. Their action at the extrinsic level is easily incoporated in the the knot type, which is changed into its mirror image. At the intrinsic level, parity is taken into account through the sign of the lower diagonal entry ϵ of the modular transformation (A1), which is also its determinant.

4. Summary

Embeddings of genus-one attractors can be classified by studying isotopy classes of the cores of the embedded tori and of their boundaries. There are three degrees of freedom by which embeddings of genus-one attractors into $\mathbb{R}^3$ can differ: knot type of extrinsic embedding, global torsion, parity (handedness).

[1] H. Whitney, Annals of Math. (2) **37**, 809 (1936).

[2] N. H. Packard, J. P. Crutchfield, J. D. Farmer, and R. S. Shaw, Phys. Rev. Lett. **45**, 712 (1980).

[3] F. Takens, Detecting strange attractors in turbulence, *Lecture Notes in Mathematics*, Vol. 898, (D. A. Rand and L.-S. Young, eds.), NY: Springer-Verlag, pp. 366-381 (1981).

[4] R. Gilmore, Revs. Mod. Phys. **70**(4), 1455 (1998).

[5] R. Gilmore and M. Lefranc, *The Topology of Chaos*, NY: Wiley-Interscience, 2002.

[6] C. Grebogi, E. Ott, and J. A. Yorke, Phys. Rev. A**37**, 1711 (1988).

[7] A. Wolf, J. B. Swift, H. L. Swinney, and J. A. Vastano, Physics D**16**, 285 (1985).

[8] H. G. Solari and R. Gilmore, Phys. Rev. A**37**, 3096 (1988).

[9] G. B. Mindlin, X.-J. Hou, H. G. Solari, R. Gilmore and N. B. Tufillaro, Phys. Rev. Lett., **64**, 2350 (1990).
[10] G. B. Mindlin, H. G. Solari, M. A. Natiello, R. Gilmore and X.-J. Hou, J. Nonlinear Sci., **1**, 147 (1991).
[11] M. Lefranc, D. Hennequin, and P. Glorieux, Physics Letters A**163**, 269 (1992).
[12] R. Brown, P. Bryant, and H. Abarbanel, Phys. Rev. A**43**, 2792 (1991).
[13] T. D. Sauer, J. A. Tempkin, and J. A. Yorke, Phys. Rev. Lett. **81**, 4341 (1998).
[14] E. N. Lorenz, J. Atmos. Sci. **63**, 130 (1963).
[15] J. Singer, Y-Z. Wang, and H. Bau, Phys. Rev. Lett. **66**, 1123 (1991).
[16] C. Letellier and G. Gouesbet, Journal de Physique II, 6, 1615 (1996).
[17] R. Gilmore and C. Letellier, *The Symmetry of Chaos*, NY: Oxford University Press, 2006.
[18] T. Ondarcuhu, G. B. Mindlin, H. L. Mancini, D. Mazza, and C. Perez-Garcia, Phys. Rev. Lett. **70**, 3892 (1993).
[19] M. Huerta, D. Krmpotic, G. B. Mindlin, H. Mancici, D. Mazza, and C. Perez-Garcia, Physics D**96**, 200 (1996).
[20] G. B. Mindlin and H. G. Solari, Phys. Rev. E**52**, 1497 (1995).
[21] T. D. Tsankov, A. Nishtala, and R. Gilmore, Phys. Rev. E**69**, 056215 1-8 (2004).
[22] T. D. Tsankov and R. Gilmore, Phys. Rev. E**69**, 056215 (2004).
[23] T. D. Tsankov and R. Gilmore, Phys. Rev. E**69**(13), 056206 (2004).
[24] M. A. Aziz-Alaoui, Int. J. Bifurcation Chaos Appl. Sci. Eng. **9**, 1009 (1999).
[25] B. Saltzman, J. Atmos. Science **19**, 327 (1962).
[26] D. Rolfsen, *Knots and Links*, Providence, RI: AMS Chelsea Publishing, 1990.
[27] O. E. Rössler, Phys. Lett. A**57**, 397 (1976).
[28] Jeffrey R. Weeks, *The Shape of Space*, Marcel Dekker, 2002.
[29] D. J. Struik, *Differential Geometry*, Reading, MA: Addison-Wesley, 1950.
[30] C. Perez and R. Gilmore (unpublished).
[31] J. S. Birman and R. F. Williams, Topology **22**, 47 (1983).
[32] J. Birman and R. F. Williams, Cont. Math. **20**, 1 (1983).
[33] G. B. Mindlin, R. Lopez-Ruiz, H. G. Solari, and R. Gilmore, Phys. Rev. E**48**, 4297 (1993).
[34] P. Grassberger and H. Kantz, Phys. Lett. A**113**, 235 (1983).
[35] M. Finardi, L. Flepp, J. Parisi, R. Holzner, R. Badii, and E. Brun, Phys. Rev. Lett. **68**, 2989 (1992).
[36] R. L. Davidchack, Y.-C. Lai, E. M. Bollt, and M. Dhamala, Phys. Rev. E**61**, 1353 (2000).
[37] Y. Hirata and K. Judd, Phys. Rev. E**70**, 016215 (2004).
[38] M. B. Kennel and M. Buhl, Phys. Rev. Lett. **91**, 084102 (2003).
[39] M. Lefranc, P. Glorieux, F. Papoff, F. Molesti, and E. Arimondo, Phys. Rev. Lett. **73**, 1364 (1994).
[40] J. Plumecoq and M. Lefranc, Physica D**144**, 231 (2000).
[41] J. Plumecoq and M. Lefranc, Physica D**144**, 259 (2000).
[42] G. Boulant, S. Bielawski, D. Derozier, and M. Lefranc, Phys. Rev. E **55**, R3801 (1997).
[43] G. Boulant, M. Lefranc, S. Bielawski, and D. Derozier, Phys. Rev. E**55**(5), 5082 (1997).
[44] G. Boulant, J. Plumecoq, S. Bielawski, D. Derozier, and M. Lefranc, in M. Dong, W. Ditto, L. Pecora, M. Spano, and S. Vohra, editors, *Proceedings of the 4th Experimental Chaos Conference*, Singapore: World Scientific, (1998), p. 121.
[45] F. Papoff, A. Fioretti, E. Arimondo, G. B. Mindlin, H. G. Solari and R. Gilmore, Phys. Rev. Lett. **68**, 1128 (1992).
[46] N. B. Tufillaro, R. Holzner, L. Flepp, R. Brun, M. Finardi, and R. Badii, Phys. Rev. A, **44**, R4786 (1991).
[47] N. B. Tufillaro, P. Wyckoff, R. Brown, T. Schreiber, and T. Molteno, Phys. Rev. E**51**(1), 164 (1995).
[48] R. Gilmore and J. W. L. McCallum, Phys. Rev. E**51**, 935 (1995).
[49] M. Lefranc and P. Glorieux, Int. J. Bifurcation Chaos Appl. Sci. Eng. **3**, 643–649 (1993).
[50] R. Gilmore, X. Pei, and F. Moss, Chaos **9**(3), 812 (1999).
[51] A. M. Fraser and H. L. Swinney, Phys. Rev. A**33**, 1134 (1986).